



Disentangling temporal and population variability in plant root water uptake from stable isotopic analysis: a labeling study

Valentin Couvreur^{1*}, Youri Rothfuss^{2*}, Félicien Meunier³, Thierry Bariac⁴, Philippe Biron⁴, Jean-Louis Durand⁵, Patricia Richard⁴, and Mathieu Javaux^{1,2}

- 5 ¹Earth and Life Institute (ELI), Université catholique de Louvain (UCL), Louvain-la-Neuve, 1348, Belgium
²Institute of Bio- and Geosciences, IBG-3 Agrosphere, Forschungszentrum Jülich GmbH, Jülich, 52425, Germany
³CAVELab - Computational & Applied Vegetation Ecology, Faculty of Bioscience Engineering, Ghent University, Campus Coupure links 653, Gent, 9000, Belgium
⁴Institute of Ecology and Environmental Sciences (IEES) – Paris, UMR 7618, CNRS-Sorbonne Université, Campus
10 AgroParisTech, Thiverval-Grignon, 78850, France
⁵UR P3F (INRA), Lusignan, 86600, France

Correspondence to: Valentin Couvreur (valentin.couvreur@uclouvain.be) and Youri Rothfuss (y.rothfuss@fz-juelich.de)

* These authors contributed equally to this work.

15 **Abstract.** Isotopic labeling techniques have the potential to minimize the uncertainty of plant root water uptake (RWU) profiles estimated through multi-source (statistical) modeling, by artificially enhancing soil water isotopic gradient. Furthermore, physical models can account for hydrodynamic constraints to RWU if simultaneous soil and plant water status data is available.

20 In this study, a population of tall fescue (*Festuca arundinacea* cv Soni) was grown in a macro-rhizotron setup under semi-controlled conditions to monitor such variables for a 34-hours long period following the oxygen stable isotopic (¹⁸O) labeling of deep soil water. Aboveground variables included tiller and leaf water oxygen isotopic compositions as well as leaf water potential (ψ_{leaf}), relative humidity, and transpiration rate. Belowground profiles of root length density (RLD), soil water content and isotopic composition were also sampled. While there were strong correlations between hydraulic variables as well as between isotopic variables, the experimental results underlined the discrepancy between variations of hydraulic and isotopic variables.

25 In order to dissect the problem, we reproduced both types of observations with a one-dimensional physical model of water flow in the soil-plant domain, for 60 different realistic RLD profiles. While simulated ψ_{leaf} followed clear temporal variations with little differences across plants as if they were “on board of the same rollercoaster”, simulated δ_{tiller} values within the plant population were rather heterogeneous (“swarm-like”) with relatively little temporal variation and a strong sensitivity to rooting depth. The physical model thus suggested that the discrepancy between isotopic and hydraulic observations was
30 logical, as the variability captured by the former was spatial and may not correlate with the temporal dynamics of the latter. For comparison purposes a Bayesian statistical model was also used to simulate RWU. While they predicted relatively similar cumulative RWU profiles, the physical model could differentiate spatial from temporal dynamics of the isotopic



signature, and supported that the local increase of soil water content and formation of a peak of labelled water observed overnight were due to hydraulic lift.

35 List of variables with symbols and units

	Leaf water potential/head:	ψ_{leaf}	in units of	MPa
	Soil water potential/head:	ψ_{soil}	in units of	MPa
	Water volumetric mass:	ρ_w	in units of	kg m^{-3}
	Soil apparent density:	ρ_b	in units of	kg m^{-3}
40	Soil gravimetric water content:	θ_{grav}	in units of	kg kg^{-1}
	Soil volumetric water content:	θ	in units of	$\text{m}^3 \text{m}^{-3}$
	Intensity of water uptake (sink term):	S	in units of	d^{-1}
	Transpiration rate per unit soil area:	T	in units of	m d^{-1}
	Air relative humidity	RH	in units of	%
45	Soil horizontal area:	A_{soil}	in units of	m^2
	Soil layer depth (for each layer):	z	in units of	m
	Soil layer thickness (for each layer):	ΔZ	in units of	m
	Root length (for each soil layer):	l_{root}	in units of	m
	Relative Root Water Uptake	rRWU	dimensionless	
50	Best run	br	dimensionless	
	Root Length Density:	RLD	in units of	m m^{-3}
	Soil water isotopic composition:	δ_{soil}	in units of	‰
	Tiller water isotopic composition:	δ_{tiller}	in units of	‰
	Leaf water isotopic composition:	δ_{leaf}	in units of	‰
55	Soil-root system conductance:	$K_{\text{soil-root}}$	in units of	$\text{m}^3 \text{MPa}^{-1} \text{s}^{-1}$
	Soil-root radial conductance:	K_{radial}	in units of	$\text{m}^3 \text{MPa}^{-1} \text{s}^{-1}$
	Root radial conductivity:	L_{pr}	in units of	$\text{m MPa}^{-1} \text{s}^{-1}$
	Root axial conductance:	K_{axial}	in units of	$\text{m}^3 \text{MPa}^{-1} \text{s}^{-1}$
	Equivalent root axial conductivity:	k_{axial}	in units of	$\text{m}^4 \text{MPa}^{-1} \text{s}^{-1}$
60	Soil hydraulic conductivity:	k_{soil}	in units of	$\text{m}^2 \text{MPa}^{-1} \text{s}^{-1}$
	Saturated soil hydraulic conductivity:	k_{sat}	in units of	$\text{m}^2 \text{MPa}^{-1} \text{s}^{-1}$



1 Introduction

65 Since the seminal work of Washburn and Smith (1934) where it was first reported that willow trees did not fractionate hydrogen stable isotopes in a hydroponic water solution during root water uptake (RWU), water stable isotopologues ($^1\text{H}^2\text{H}^{16}\text{O}$ and $^1\text{H}_2^{18}\text{O}$) have been used as indicators for plant water sources in soils. In their review, Rothfuss and Javaux (2017) reported in the period 2015-2016 about no less than 40 publications in which RWU was retrieved from stable isotopic measurements. Novel measuring techniques (e.g., cavity ring-down spectroscopy – CRDS and off-axis integrated cavity output spectroscopy – ICOS) providing ways for fast and cost-effective water stable isotopic analyses certainly enable and
70 emulate current research in that field. Water stable isotopologues are no longer powerful tracers waiting for technological developments (Yakir and Sternberg, 2000) but are on the verge to be used to their full potential for addressing eco-hydrological research questions and identify processes in the soil-plant-atmosphere continuum (Werner et al., 2012; Dubbert and Werner, 2019; Sprenger et al., 2016).

The isotopic determination of RWU profiles is based on the principle that the isotopic composition of xylem water at the
75 outlet of the root system (i.e., in the first aerial and non-transpiring node of the plant) equals the mean value of the soil water isotopic composition across contributing sources, weighted by their relative contribution to RWU. Results come only with reasonable precision when (i) the soil water isotopic composition depth gradient is strong and (ii) the temporal dynamics of RWU and soil water isotopic composition is relatively low. Condition (i) is fulfilled mostly at the surface of the soil, while soil water isotopic composition gradients become usually lower or null with increasing depth (due to the isotopic influence
80 of the groundwater table). Condition (ii) is often neglected but is required due to the instantaneous nature of the sap flow samples. As illustrated by Oerter and Bowen (2019), the lateral variability of the soil water isotopic composition profiles can become significant in the field and could have great implications on the representability and meaningfulness of isotopic-derived estimate of RWU profiles.

To overcome these limitations, labeling pulses have been increasingly used in recent works to artificially alter the natural
85 isotopic gradients (e.g., Beyer et al., 2016; Beyer et al., 2018; Grossiord et al., 2014; Jesch et al., 2018; Volkmann et al., 2016). However, a precise characterization of the artificial spatial (i.e., lateral and vertical) and temporal distributions of the soil water isotopic composition (driven by e.g., soil isotopic water flow) is crucial. The punctual assessments of the isotopic composition profiles following destructive sampling in the field and subsequent extraction of water in the laboratory might neither be spatially nor temporally representative and can lead to erroneous estimates of RWU profiles (Orlowski et al.,
90 2018; Orlowski et al., 2016).

The vast majority of isotopic studies use statistical (e.g., Bayesian) modeling to retrieve RWU profile solely from the isotopic composition of water extracted in the soil and the shoot (Rothfuss and Javaux, 2017). However, when data on soil and plant water status is available, hydraulic modeling tools can also be used to connect different data types in a process-based manner and estimate root water uptake profiles (Passot et al., 2019). Some of the most simplistic models use 1-D
95 relative root distribution and plant-scale hydraulic parameters (Sulis et al., 2019), while the most complex rely on root



architectures and root segment permeabilities (Meunier et al., 2017c). Only a handful of studies coupled isotopic measurements in plant tissues and soil material with models describing RWU in a mechanistic manner. For instance, Meunier et al. (2017a) could both locate and quantify the volume of redistributed water by *Lolium multiflorum* by labeling of the soil with ^{18}O enriched water under controlled conditions.

100 Building on the work of Meunier et al. (2017a), the objective of the present study is to investigate on the plant and environmental factors that affect the tiller xylem water isotopic composition in a population of *Festuca arundinacae* cv Soni. (tall fescue), in order to unveil pitfalls and opportunities in methods used to predict RWU profiles from stable isotopic analyses following a labeling pulse.

2 Material and methods

105 Our experiment consisted in supplying labeled water from the bottom to a macro-rhizotron in which tall fescue was grown. Data on soil and plant isotopic signature and hydraulic status were monitored for 34 hours. In the following, the oxygen isotopic composition of water will be expressed in per mil (‰) on the “delta” ($\delta^{18}\text{O}$) scale with respect to the international water standard V-SMOW (Gonfiantini, 1978).

2.1 Rhizotron experimental setup

110 The macro-rhizotron (dimensions: 1.6 m x 1.0 m x 0.2 m, see picture in Appendix A) was placed inside a glasshouse (INRA Lusignan, France), where it was continuously weighed (KE1500, Mettler-Toledo, resolution: 20 g) to monitor water effluxes (i.e., bare soil evaporation or evapotranspiration). Underneath the soil compartment and in contact with it, a water reservoir (height: 0.1 m) filled with gravel acted as water table and allowed the supply of water to the rhizotron. The rhizotron was equipped with two sets of CS616 water content reflectrometer profiles (Campbell Scientific, USA) with 30 cm long probe
115 rods positioned at six depths (−0.05, −0.10, −0.30, −0.60, −1.05 and −1.30 m) and one profile of tensiometers (SMS 2000, SDEC-France) located at four depths (−0.05, −0.10, −0.30, and −0.60 m) in order to monitor the evolutions of soil water volumetric content (θ , in $\text{m}^3 \text{m}^{-3}$) and matric potential. Finally, relative humidity (RH, %) was recorded above the vegetation with one humidity and temperature probe (HMP45D, Vaisala, Finland). The transparent polycarbonate sides (front and back) allowed the daily observations of root maximal depth. The experimental setup allowed precisely controlling the amount and
120 $\delta^{18}\text{O}$ of soil input water. Another important feature was the soil depth (i.e., 1.60 m) which minimized the influence of the water table on superficial layers water content and $\delta^{18}\text{O}$.

2.2 Soil properties and installation

The soil is classified as District Cambisol (particle size distribution: sand 15%, silt 65%, clay 20%) with a dry bulk density of $\rho_b = 1420 \text{ kg m}^{-3}$. Prior installation in the rhizotron, the substrate was sieved at 2 mm and dried out in an air oven at 110
125 °C during 48 h to remove most of the residual water. 450 kg of soil were installed in the rhizotron by layer of 0.10 m and



compacted in order to reach the above-mentioned value of dry bulk density. Soil water retention data was derived from synchronous measurements of soil water content (CS616 soil water reflectometers, Campbell Scientific, USA) and potential (Sols – PST55 micro-psychrometers, WESCOR, and SMS 2000 tensiometers, SDEC) from saturated to residual water content. The closed-form water retention curve (van Genuchten, 1980) was then parametrized by minimizing the root mean square difference between its position and measured soil water content-potential couples (Appendix B).

2.3 Experimental protocol

After installation, the soil was gradually flooded with local water ($\delta^{18}\text{O} = -6.8\text{‰}$) from the bottom reservoir up to the top of the profile for a period of three days in order to reduce as much as possible the initial lateral and vertical heterogeneities in water content and $\delta^{18}\text{O}$. The tall fescue (*Festuca arundinaceae* cv Soni) was sown at a seeding density of 3.6 g m^{-2} (which corresponds for the rhizotron surface area of 0.2 m^2 to roughly 300 plants) when soil water content reached $0.25\text{ m}^3\text{ m}^{-3}$ (corresponding to pF 2.3) at -0.05 m , as measured by the soil water sensors, and emerged 12 days later.

166 days after seeding (DaS 166) the following conditions were fulfilled: (i) there was a strong soil water content gradient between the soil deep [-1.5 m , -1.0 m] and superficial [-0.3 m , 0 m] layers, (ii) the tall fescue roots had reached a depth of -1.5 m (observed through polycarbonate transparent slides). That same day at 17:00, the reservoir's water was labelled and its isotopic composition measured at $+470\text{‰}$. Soil was sampled on four occasions from the surface down to -1.3 m : before labeling (DaS 166 - 15:45) and after labeling on DaS 167 - 07:00, DaS 167 - 17:00 and DaS 168 - 05:00 for the determination of soil gravimetric water content (θ_{grav} , in kg kg^{-1}) and isotopic composition (δ_{soil} , in ‰). Gravimetric water content was then converted to volumetric water content ($\theta = \theta_{\text{grav}} * \rho_b / \rho_w$, in $\text{m}^3\text{ m}^{-3}$, where ρ_b is the bulk soil density and ρ_w is the water density). On 40 occasions during a 34-hour long period three plants were sampled from the vegetation (i.e., 120 plants were sampled in total from the cover). Each plant's tillers and leaves were pooled into two separate vials. Dead material as well as the oldest living leaf around each tiller were removed in order not to contaminate tiller samples with transpiring material (Durand et al., 2007). In addition, air water vapor was collected from the atmosphere of the surrounding of the rhizotron. The air was run at a flow rate of 1.5 l min^{-1} through two glass cold traps in series immersed in a mixture of dry ice and pure ethanol at -80°C . Water from tillers, leaves, and soil samples were extracted by vacuum distillation and their isotopic compositions (i.e., δ_{tiller} , δ_{leaf} , and δ_{soil}) together with that of atmospheric water vapor (δ_{atm}) were measured with an IRMS (Isoprep 18 - Optima, Fison, Great-Britain, precision accuracy of 0.15‰). Finally, leaf water potential (ψ_{leaf} , in MPa) was monitored with a pressure chamber on two leaves per sampled plant, and transpiration (T , m d^{-1}) was derived from the changes in mass of the rhizotron at the same temporal scale as plant sampling.

Root biomass was determined from the horizontal sampling of soil between the polycarbonate sides using a 2 cm diameter auger at -0.02 , -0.08 , -0.10 , -0.40 , -0.55 , -0.70 , -0.90 , -1.10 , and -1.30 m soil depth. Each depth was sampled once to thrice. Each soil core was washed of soil particles and roots were collected over a 0.2 mm mesh filter, and dried at 60°C for 48 hours. Finally, Root Length Density (RLD, in $\text{m root (m soil)}^{-3}$) distribution was determined from the root dry mass using the specific root length determined by Gonzalez-Dugo et al. (2005) specifically for tall fescue ($95\text{ m root (g root)}^{-1}$). The



160 reader is referred to Appendix C for an overview of the type and timing of the different destructive measurements during the intensive sampling period.

2.4 Modeling of RWU and δ_{filler}

60 tall fescue root systems with rooting depths ranging from -1.30 to -1.60 m depth (based on our own observations and those of the literature, e.g., Schulze et al., 1996; Fan et al., 2016) were modeled to represent the community in the rhizotron. The root systems were generated with the root architecture simulator CRootBox (Schnepf et al., 2018) so that the simulated RLD matched observations (Fig. 1a). Each simulated root system was considered as representative of a “class” among the plant population. Each root system class was assumed to occupy one sixtieth of the total horizontal area. To simulate RWU by the 60 classes while limiting the computing time in the inverse modeling scheme, we considered each of them as a “big root” hydraulic network with equivalent radial and axial hydraulic conductances (thus neglecting architectural aspects but accounting for their respective root length density profiles).

170 The radial soil-root conductance between the bulk soil and each class’s (i) root surface in soil layer j ($K_{\text{radial},j}$, $\text{m}^3 \text{MPa}^{-1} \text{d}^{-1}$) was assumed as variable in time (t):

$$K_{\text{radial},i,j}(t) = \frac{2\pi r_{\text{root}} l_{\text{root},i,j} B_j L_{\text{pr}} k_{\text{soil},j}(t)}{B_j k_{\text{soil},j}(t) + r_{\text{root}} L_{\text{pr}}} \quad (1)$$

with B (dimensionless) a geometrical factor approximating the dimension of the domain between the bulk soil and root surface as radial, as given by Schroeder et al. (2009):

$$175 \quad B_j = \frac{2(1-\rho_j)(1+\rho_j)}{2\rho_j^2 \ln \rho_j - \rho_j^2 + 1} \quad (2)$$

where ρ (dimensionless) represents the ratio of the distance between roots and the root averaged diameter. The averaged distance between roots can be deduced from the observed root length density (RLD_j , m m^{-3}) and root radius (r_{root} , m):

$$\rho_j = \frac{\sqrt{\frac{1}{\pi \text{RLD}_j}}}{r_{\text{root}}} \quad (3)$$

In Eq. (1), the soil hydraulic conductivity function of Mualem (1976) and van Genuchten (1980) was used:

$$180 \quad k_{\text{soil},j}(t) = k_{\text{sat}} \cdot Se_j^\lambda(t) \left(1 - \left(1 - Se_j^{\frac{1}{m}} \right)^m \right)^2 \quad (4)$$

where k_{sat} ($\text{m}^2 \text{MPa}^{-1} \text{d}^{-1}$), m (dimensionless) and λ (dimensionless) are soil hydraulic parameters (with $m = 1 - 2/n$) and Se_j , the relative water content (dimensionless), is computed from the saturated (θ_{sat} , $\text{m}^3 \text{m}^{-3}$) and residual (θ_{res} , $\text{m}^3 \text{m}^{-3}$) water contents as:

$$Se_j = \frac{\theta_j - \theta_{\text{res}}}{\theta_{\text{sat}} - \theta_{\text{res}}} \quad (5)$$

185 The last term to define in Eq. (1) is the root length in each soil layer (l_{root} , m). Unlike the geometrical parameter B , which defines a domain geometry between the bulk soil and roots of the overall population, the l_{root} term is class specific (i) and uses the simulated root length density profiles over an area corresponding to one sixtieth of the total setup horizontal area:



$$l_{\text{root},i,j} = \frac{\Delta Z_j \cdot A_{\text{soil}} \cdot \text{RLD}_{i,j}}{60} \quad (6)$$

with ΔZ (m) and A_{soil} (m^2) the soil layer thickness and horizontal surface area, respectively.

190 To finalize the connection between root xylem and shoot, axial conductances per root system class (K_{axial} , $\text{m}^3 \text{MPa}^{-1} \text{d}^{-1}$) were derived from an equivalent “big root” specific axial conductance per root system class (k_{axial} , $\text{m}^4 \text{MPa}^{-1} \text{d}^{-1}$) as:

$$K_{\text{axial},j} = \frac{k_{\text{axial}}}{\Delta Z_j} \quad (7)$$

At each time step, both the total soil-root system conductance ($K_{\text{soil-root}}$, $\text{m}^3 \text{MPa}^{-1} \text{d}^{-1}$) and the standard sink distribution (SSF , dimensionless, summing up to 1) were calculated from K_{radial} and K_{axial} , using the algorithm of Meunier et al. (2017b).

195 The variable $K_{\text{soil-root}}$ represents the water flow per unit water potential difference between the bulk soil and the leaf (assuming a negligible stem hydraulic resistance), and SSF the relative distribution of water uptake in each soil layer under vertically homogeneous soil water potential conditions (Couvreur et al., 2012).

Adding soil hydraulic conductance to the one-dimensional hydraulic model of Couvreur et al. (2014) yields the following solutions of leaf water potential (ψ_{leaf} , MPa) and water sink terms (S , d^{-1}) whose formulation approaches that of Nimah and

200 Hanks (1973):

$$\psi_{\text{leaf}}(t) = -\frac{T(t)}{K_{\text{soil-root}}(t)} + \sum SSF_j(t) \cdot \psi_{\text{soil},j}(t) \quad (8)$$

Where one sixtieth of the overall transpiration rate (T) is allocated to each class, and $\psi_{\text{soil},j}$ (Mpa) is the soil water potential in soil layer j .

$$S_{i,j}(t) = \frac{K_{\text{soil-root},i}(t) \cdot SSF_{i,j}(t) \cdot (\psi_{\text{soil},j}(t) - \psi_{\text{leaf},i}(t))}{A_{\text{soil}} \cdot \Delta Z_j} \quad (9)$$

205 where axial conductances were assumed to be large enough for $K_{\text{soil-root}}$ to control the compensatory RWU which arise from a heterogeneously distributed soil water potential (Couvreur et al., 2012).

Finally, the tiller water isotopic composition (δ_{tiller}) was calculated as the average of local soil water isotopic compositions (δ_{soil}) weighted by the relative distribution of positive water uptakes (i.e., not accounting for δ_{soil} at locations where water is exuded by the root), assuming a perfect mixture of water inside the root system (Meunier et al., 2017a):

$$210 \quad \delta_{\text{tiller}} = \frac{\sum_{S_j > 0} S_j \cdot A_{\text{soil}} \cdot \Delta Z_j \cdot \delta_{\text{soil}}(t)}{\sum_{S_j > 0} S_j(t) \cdot A_{\text{soil}} \cdot \Delta Z_j} \quad (10)$$

Like in the experiment, δ_{tiller} from three plants were randomly pooled at each observation time. As the experiment included about 300 plants (value based on seeding density, see section 2.3), and we explicitly simulated 60 individual RLD profiles, we assumed that each of them was representative of a class of 5 identical plants, totaling 300 plants. A hundred pools of 3 plants (possibly including several plants of the same class) were randomly selected in order to obtain the pooled simulated

215 δ_{tiller} by arithmetic averaging.

The unknown parameters of the soil-root hydraulic model, i.e., the root radial conductivity (L_{pr}), the root axial conductance (k_{axial}), the soil saturated hydraulic conductivity (k_{sat}), and the soil tortuosity factor (λ) were finally determined by inverse modeling. For details on the procedure, the reader is referred to Appendix D.



220 In order to evaluate the robustness of the hydraulic model predictions (parametrized solely based on the reproduction of
shoot observations in the inverse modeling scheme) from independent perspectives, we also compared predictions and
measurements over 4 quantitative “soil-root domain” criteria: (i) the depth at which the transition between nighttime water
uptake and exudation takes place, (ii) quantities of exuded water and overnight increase of soil water content, (iii) the
enrichment of labelled water at the depth where water content increase is observed overnight, and (iv) the order of magnitude
of the optimal root radial conductivity value as compared to literature data in tall fescue.

225 Finally, and as a comparison point, the Bayesian inference statistical model SIAR (Parnell et al., 2013) was used to
determine the profiles of water sink terms of ten identified potential water sources. These water sources were defined to
originate from 10 distinct soil layers for which corresponding δ_{soil} values were computed (Rothfuss and Javaux, 2017). SIAR
solely bases its estimates from the comparison of δ_{tiller} observations to the isotopic compositions of the soil water sources
(δ_{soil}). For this, δ_{tiller} measurements were pooled in twelve groups corresponding to different time periods, selected to best
230 reflect the observed temporal dynamics of δ_{tiller} . The reader is here referred to Appendix E for details on the model
parametrization and running procedure.

3 Results and discussion

3.1 Experimental data

3.1.1 Soil profiles

235 Figure 2a and b show a very stable soil water content profile and a more variable δ_{soil} profile from DaS 166 - 15:45 to DaS
168 - 05:00. Soil was dry at the surface ($0.058 \text{ m}^3 \text{ m}^{-3} < \theta < 0.092 \text{ m}^3 \text{ m}^{-3}$ for layer 0.015 - 0.040 m) whereas closer to
saturation at depth -1.30 m ($\theta = 0.34 \text{ m}^3 \text{ m}^{-3} \pm 0.012 \text{ m}^3 \text{ m}^{-3}$, estimated $\theta_{\text{sat}} = 0.40 \text{ m}^3 \text{ m}^{-3}$, see Appendix A). According to
the measured soil matric potentials (Fig. 2c), soil water was virtually unavailable ($\leq -1.5 \text{ MPa}$) above -0.5 m depth. Soil
moisture remained unchanged in the top 25 cm during the sampling period ($\theta = 0.08 \pm 0.00 \text{ m}^3 \text{ m}^{-3}$) while varied noticeably
240 at -1.3 m between 12:00 and 20:00 on DaS 167 ($0.33 \pm 0.01 \text{ m}^3 \text{ m}^{-3}$), showing that roots were predominantly extracting
water from deep soil layers. Water in the top soil layers ($-0.040 \text{ m} < z < -0.015 \text{ m}$) was isotopically enriched ($-3.2 \text{ ‰} < \delta_{\text{soil}}$
< 0.3 ‰) as opposed to the deepest layer ($\delta_{\text{soil}} = -7.34 \text{ ‰} \pm 0.30 \text{ ‰}$ at 1.30 m). Following labeling of the reservoir water on
DaS 166 - 17:00, δ_{soil} reached a value of 36.9 ‰ at -1.50 m on DaS 167 - 07:30. The development of the vegetation on DaS
166-168 (LAI = 5.6) and the observed surface θ values lead to assume that the rhizotron water losses were due to
245 transpiration flux solely (i.e., evapotranspiration = transpiration). The soil water isotopic exponential-shaped profiles were
the product of fractionating evaporation flux, and to a great extent when the soil was bare or when the tall fescue cover was
not fully developed. The differences in soil water isotopic profile observed at the four different sampling dates were
therefore either due to lateral heterogeneity (e.g., upper soil layers), to the soil capillary rise of labelled water from the
reservoir (deep soil layers), or to the hydraulic redistribution of water through roots. The observed RLD profile (Fig. 1a)



250 showed a typical exponential shape, i.e., maximal at the surface ($5.42 \pm 0.34 \text{ cm cm}^{-3}$) down to a minimal at -1.10 m ($0.540 \pm 0.35 \text{ cm cm}^{-3}$), while it increased again from the latter depth up to a value of 1.660 cm cm^{-3} at -1.30 m . This significant trend was most probably a direct consequence of the high soil water content level in this deeper layer.

3.1.2 Plant water and isotopic temporal dynamics

The temporal variation of δ_{tiller} (Fig. 3a) was found to be either (i) moderate during day and night, i.e., from DaS 167 - 06:00 to 11:00 ($\delta_{\text{tiller}} = -2.6 \pm 1.4 \text{ ‰}$) and from DaS 167 - 21:30 to DaS 168 - 00:00 ($\delta_{\text{tiller}} = -2.7 \pm 0.4 \text{ ‰}$), or (ii) strong during the day, i.e., from DaS 167 - 11:00 to 18:00 (maximum value of 20.9 ‰ at DaS 167 - 12:40), or else (iii) strong during the night, i.e., from DaS 167 - 04:00 to 06:00 (max = 36.4 ‰ at DaS 167 - 05:15) and from DaS 168 - 00:00 to 06:00 (max = 14.6 ‰ at 28:00, DaS 168). Note that transpiration (Fig. 3b) occurred also at night during the sampling period, due to relatively high temperature in the glasshouse leading to a value of atmospheric relative humidity smaller than 85% , Fig. 3b). From 12:00 to 14:00 and from 16:00 to 17:00 on DaS 167 (case (ii)) high values of leaf transpiration corresponded to high values of δ_{tiller} .

3.1.3 Partial decorrelation between water and isotopic state variables

Figure 4 shows that variables describing plant water status, i.e., T and RH (Fig. 4a) and T and ψ_{leaf} (Fig. 4b) were well correlated: coefficient of determination R^2 was equal to 0.78 and 0.70 for the entire experimental duration, respectively. However, linear relationships between water status and isotopic variables were either inexistent, e.g., between T and δ_{tiller} ($R^2=0.01$, Fig. 4c) and between ψ_{leaf} and δ_{tiller} ($R^2=0.00$, Fig. 4h) or characterized by a low R^2 and high p-value (e.g., between T and δ_{leaf} , $R^2=0.43$, $p>0.05$, Fig. 4d). The partial temporal disconnection between δ_{leaf} and T could not be attributed to problems of the isotopic methodology, during e.g., the vacuum distillation of the water from the plant tillers and leaves: water recovery rate was always greater than 99% and Rayleigh distillation corrections were applied to standardize the observed isotopic composition values to a 100% water recovery (based on the comparison of sample weight loss during distillation and mass of collected distilled water). The evolution of δ_{leaf} was strongly correlated with that of δ_{tiller} during the day ($R^2 = 0.90$) whereas non-correlated during the night ($R^2 = 0.00$, Fig. 4j). These observed correlations are in agreement with the Craig and Gordon (1965) model revisited by Dongmann (1974) and extensively used in the current literature (e.g., Dubbert et al., 2017): at isotopic steady-state, δ_{leaf} is a function of the input water isotopic composition (δ_{tiller}) among other variables, i.e., leaf temperature (not measured during the experiment), stomatal and boundary layer conductances, isotopic composition of atmospheric water vapor, and relative humidity.

It is generally difficult to observe a statistically significant $\delta_{\text{leaf}}-\delta_{\text{tiller}}$ (Fig. 4j) relationship at this temporal scale under natural abundance conditions in the field since the soil water isotopic weak gradient translates into weaker δ_{tiller} temporal dynamics. The quality of linear fit between δ_{leaf} and δ_{tiller} data collected during the day ($R^2=0.90$) was made possible in this specific experiment by the artificial isotopic labeling pulse that enhanced the soil water isotopic gradient, which in turn increased the range of variation of δ_{tiller} , ultimately highlighting the $\delta_{\text{leaf}}-\delta_{\text{tiller}}$ temporal correlation. Air relative humidity is a driving variable of δ_{leaf} in the model of Dongmann (1974) via the competing terms $(1-\text{RH})\cdot\delta_{\text{tiller}}$ et $\text{RH}\cdot\delta_{\text{atm}}$, where δ_{atm} is the



atmospheric water vapor isotopic composition inside the glasshouse. An overall significant linear correlation was observed between RH and δ_{leaf} during the experiment ($R^2=0.57$, Fig. 4g). During the two night periods (i.e., from 04:00-06:00 and from 20:30-07:00), as relative humidity increased in the glasshouse ($51 \% < \text{RH} < 85 \%$, Fig. 3b), the influence of the isotopic labeling of the tiller water (due to the labeling of deep soil water) through term $(1-\text{RH})\cdot\delta_{\text{tiller}}$ decreased to the benefit of term $\text{RH}\cdot\delta_{\text{atm}}$ (with δ_{atm} values ranging from -15.9 to -10.7% , mean = $-13.1\pm 1.6\%$, data not shown). This was especially visible between 04:50 and 06:00 on DaS 167 and between 01:00 to 06:00 on DaS 168, when δ_{tiller} reached greater values than δ_{leaf} .

From a different perspective, as three plant water samples were pooled to reach a workable volume for the isotopic analysis at each observation time without replicates, the isotopic signal fluctuations may reflect both its temporal dynamics and its variability within the plant population.

3.2 Simulations

3.2.1 Rooting depth and transpiration rate control δ_{tiller} and ψ_{leaf} fluctuations, respectively

Despite the use of a global optimizer and 4 degrees of freedom (L_{pr} , k_{axial} , k_{sat} , λ , see optimal values in Table 1) specifically aiming at matching the simulated and observed temporal dynamics of δ_{tiller} , none of the 60 root system classes or average population could reproduce the measured fluctuations in time ($R^2=0.00$, Fig. 5a), regardless of the weight attributed to this criterion in the objective function. However, the predicted versus observed average δ_{tiller} and its standard deviation for the overall dataset were not significantly different ($6.6 \pm 8.4 \%$ and $3.7 \pm 8.4 \%$, respectively). Besides, the simulated ψ_{leaf} fitted well the observations ($R^2=0.67$, overall distributions: -0.175 ± 0.053 MPa and -0.177 ± 0.053 MPa, respectively, Fig. 5c). When analyzing the distributions of ψ_{leaf} and δ_{tiller} per maximum root system depth (Fig. 5b and d), it appears that the ψ_{leaf} signal is not sensitive to the rooting depth (Fig. 5d), while δ_{tiller} is more sensitive to rooting depth than to the temporal evolution of the plant environment (Fig. 5b).

This leaves us with two hypotheses. The “rollercoaster hypothesis”: δ_{tiller} rapidly goes up and down with all the population on board of the same car (i.e. little variability within the population, unlike predictions in Fig. 5a, but like the simulated ψ_{leaf} in Fig. 5c). If that is correct, the physical model lacks a process that would capture the observed temporal fluctuations of δ_{tiller} . The “swarm pattern hypothesis”: δ_{tiller} is rather stable in time but its values within the plant population are dispersed like in a flying swarm, so that δ_{tiller} values sampled at different times fluctuate, not due to temporal dynamics but to the fact that different individuals are sampled (Fig. 5a).

The model suggests that the tall fescue population ψ_{leaf} follows a “rollercoaster” dynamics driven by transpiration rate, while the population δ_{tiller} follows a “swarm” pattern driven by the maximum rooting depth of the sampled plants. As no correlation could be expected between the drivers, transpiration rate and the maximum rooting depth of the sample plants, discrepancies between fluctuations of isotopic and hydraulic variables are not surprising any more.



In future experiments and in the specific context of labeling pulses, sampling more plants at each observation time would help disentangle the spatial from temporal sources of variability of ψ_{leaf} and δ_{tiller} . It would however be at the cost of the temporal resolution of observations, or would necessitate a larger setup with more plants in the case of controlled conditions experiments.

3.2.2 Independent observations support the validity of the hydraulic model predictions

In the last 12 hours of the experiment (DaS 167 – 17:00 to DaS 168 – 05:00), the measured soil water content increased by 2.9% at –0.9 m depth, which could be a sign of nighttime hydraulic redistribution. During the same period, the physical model predicted a cumulative water exudation sufficient to increase soil water content by 0.38 %, as soil water potential was sufficiently low to generate reverse flow, but high enough not to disrupt the hydraulic continuity between soil and roots (Carminati and Vetterlein, 2013; Meunier et al., 2017a). While this increase is smaller than the observed water content change, it is only a component in the soil water mass balance. Given the soil water potential vertical gradient, upward soil capillary water flow may have accounted for another part of the observed moisture change. Experimental observations also show that δ_{soil} increased by 1.0 ‰ at 0.9 m depth during that time (–6.2 ‰, a value significantly higher than $-7.1 \text{ ‰} \pm 0.1 \text{ ‰}$ at earlier times), while our simulations of hydraulic redistribution generated an increase of δ_{soil} by 0.41 ‰. As soil capillary flow may not generate local maxima of δ_{soil} (no enrichment observed at surrounding heights, see Fig. 2b), and soil evaporation is assumed negligible at that depth, it is likely that the observed local enrichment was entirely due to hydraulic redistribution, which would then be underestimated by a factor of about 2.5 in our simulations. Increasing water exudation by a factor 2.5 would imply a simulated water content change due to exudation of 0.95% absolute water content, which remains compatible with the experimental observation.

Between –1.1 m and –0.9 depth, the nighttime water flow pattern transitioned from exudation to uptake in both measurements and predictions. At –1.1 m, the model predicted a cumulative water uptake sufficient to decrease soil water content by 0.89 %, as compared to the observed 1.41 % total soil water content decrease. The remaining 0.5% water content decrease may have contributed to the recharge to the soil layers above through capillary flow, which was not simulated.

The fitted L_{pr} value ($2.3 \cdot 10^{-7} \text{ m MPa}^{-1} \text{ s}^{-1}$) was in the range found by Martre et al. (2001) in tall fescue ($2.2 \cdot 10^{-7} \pm 0.1 \text{ m MPa}^{-1} \text{ s}^{-1}$) and falls in the range obtained by Meunier et al. (2017a) for another grass (*Lolium multiflorum* Lam., $6.8 \cdot 10^{-8}$ to $6.8 \cdot 10^{-7} \text{ m MPa}^{-1} \text{ s}^{-1}$). Our k_{axial} value cannot be compared to values of axial root conductance from the literature as it transfers the water absorbed by roots from 5 plants in a single “big root” per class of root system. The optimal value of k_{sat} was quite high (Table 1) but reportedly very correlated to λ , so that the low value of the latter compensated the high value of the former, thus they should be considered as effective rather than physical parameters.

3.2.3 Do root water uptake profiles predicted by hydraulic and Bayesian models differ?

The root water uptake dynamics predicted by the mechanistic model are shown in Fig. 6a. The overall pattern of peaking water uptake in the lower part of the profile during daytime matched that of the statistical model, and the correlation



345 coefficient of both models predictions was relatively high ($R^2=0.53$) in average over the simulation period, see Figure of
Appendix E). The main differences were the following: (i) in the upper soil layers where the soil water potential was lower –
1.5 MPa, the statistical model predicted water uptake, which is theoretically impossible given the leaf water potential above
–0.4 MPa (van Den Honert, 1948); (ii) In the top half of the profile, the physical model predicted exudation at a rate limited
by the low hydraulic conductivity between root surface and bulk soil, with a peak at night, at –0.9 m depth (quantitative
analysis in previous section); (iii) Below –1.0 m depth, the water uptake rate predicted by the statistical model steadily
350 increased with depth while that of the physical model was more uniform, likely due to axial hydraulic limitation (e.g., Bouda
et al., 2018) counteracting the increasing soil water potential with depth.

4 Conclusion

In the present study, light could be shed on RWU of *Festuca arundinacae* by specifically manipulating the lower boundary
355 conditions for water content and oxygen isotopic composition. The new version of the one-dimensional model of Couvreur
et al. (2014) implemented here accounted for both root and soil hydraulics in a population of “big” root systems of known
root length density profile. This approach underlined the high sensitivity of δ_{tiller} to rooting depth and suggested that if δ_{tiller} is
measured on a limited number of individuals, its variations in time may reflect the heterogeneity of rooting depth within the
population, rather than temporal dynamics which was minor in our simulations. The model avoided the prediction of water
360 uptake at locations where it was physically unavailable (e.g., in the first half of the soil profile), by accounting for water
potential differences observed between the leaves and the soil, and explained quantitatively the local isotopic enrichment of
soil water as the occurrence of nighttime Hydraulic Lift at –0.9 m depth. On the other hand, the Bayesian statistical approach
tested for comparison, which was driven by isotopic information solely, naturally translated the observed changes of δ_{tiller}
into profound temporal dynamics of RWU, at the expense of eco-physiological consideration (e. g., temporal dynamics of
365 leaf water potential and transpiration rate).

This case study highlights (i) the potential limitations water isotopic labeling techniques for studying RWU, especially when
water addition is localized and not broadcasted in the soil therefore creates strong isotopic depth-gradients. As already
pointed out in the review of Rothfuss and Javaux (2017), the study also (ii) underlines the interest of complementing in-situ
isotopic observations in soil and plant water with information on soil water status and plant eco-physiology; it finally (iii)
370 calls for the use of simple soil-root models for inverting isotopic data and gain insights into the RWU process.



Acknowledgements

The experimental part of this study was financed by the French national scientific program EC2CO/CITRIX.

Data sets

375 Upon acceptance, all research data needed for creating plots will be available in reliable FAIR-aligned data repositories with assigned DOIs.

Author contribution

TB, JLD, and PB designed the experiments and TB, JLD, PB, and YR carried them out. VC and FM developed the physically-based root water uptake model code and performed the simulations. YR performed the statistical simulations. VC
380 and YR prepared the manuscript with contributions from all co-authors.

Competing interests

The authors declare that they have no conflict of interest.



385 **References**

- Beyer, M., Koeniger, P., Gaj, M., Hamutoko, J. T., Wanke, H., and Himmelsbach, T.: A deuterium-based labeling technique for the investigation of rooting depths, water uptake dynamics and unsaturated zone water transport in semiarid environments, *J. Hydrol.*, 533, 627-643, doi:10.1016/j.jhydrol.2015.12.037, 2016.
- Beyer, M., Hamutoko, J. T., Wanke, H., Gaj, M., and Koeniger, P.: Examination of deep root water uptake using anomalies of soil water stable isotopes, depth-controlled isotopic labeling and mixing models, *J. Hydrol.*, 566, 122-136, doi:10.1016/j.jhydrol.2018.08.060, 2018.
- 390 Bouda, M., Brodersen, C., and Saiers, J.: Whole root system water conductance responds to both axial and radial traits and network topology over natural range of trait variation, *J. Theor. Biol.*, 456, 49-61, doi:10.1016/j.jtbi.2018.07.033, 2018.
- Carminati, A., and Vetterlein, D.: Plasticity of rhizosphere hydraulic properties as a key for efficient utilization of scarce resources, *Ann. Bot.*, 112, 277-290, doi:10.1093/aob/mcs262, 2013.
- 395 Couvreur, V., Vanderborght, J., and Javaux, M.: A simple three-dimensional macroscopic root water uptake model based on the hydraulic architecture approach, *Hydrol. Earth Syst. Sc.*, 16, 2957-2971, doi:10.5194/hess-16-2957-2012, 2012.
- Couvreur, V., Vanderborght, J., Beff, L., and Javaux, M.: Horizontal soil water potential heterogeneity: simplifying approaches for crop water dynamics models, *Hydrol. Earth Syst. Sc.*, 18, 1723-1743, doi:10.5194/hess-18-1723-2014, 2014.
- 400 Craig, H., and Gordon, L. I.: Deuterium and oxygen 18 variations in the ocean and marine atmosphere, *Stable Isotopes in Oceanographic Studies and Paleotemperatures*, Spoleto, Italy, 1965, 9-130, 1965.
- Dongmann, G.: Contribution of Land Photosynthesis to Stationary Enrichment of O-18 in Atmosphere, *Radiat. Environ. Biophys.*, 11, 219-225, doi:10.1007/Bf01323191, 1974.
- Dubbert, M., Kübert, A., and Werner, C.: Impact of Leaf Traits on Temporal Dynamics of Transpired Oxygen Isotope Signatures and Its Impact on Atmospheric Vapor, *Frontiers in Plant Science*, 8, 5, doi:10.3389/fpls.2017.00005, 2017.
- 405 Dubbert, M., and Werner, C.: Water fluxes mediated by vegetation: emerging isotopic insights at the soil and atmosphere interfaces, *New Phytol.*, 221, 1754-1763, doi:10.1111/nph.15547, 2019.
- Durand, J. L., Bariac, T., Ghesquière, M., Biron, P., Richard, P., Humphreys, M., and Zwierzykowski, Z.: Ranking of the depth of water extraction by individual grass plants using natural ¹⁸O isotope abundance, *Environ. Exp. Bot.*, 60, 137-144, 2007.
- 410 Fan, J. L., McConkey, B., Wang, H., and Janzen, H.: Root distribution by depth for temperate agricultural crops, *Field Crops Res.*, 189, 68-74, doi:10.1016/j.fcr.2016.02.013, 2016.
- Gonfiantini, R.: Standards for stable isotope measurements in natural compounds, *Nature*, 271, 534-536, doi:10.1038/271534a0, 1978.
- Gonzalez-Dugo, V., Durand, J. L., Gastal, F., and Picon-Cochard, C.: Short-term response of the nitrogen nutrition status of tall fescue and Italian ryegrass swards under water deficit, *Aust. J. Agric. Res.*, 56, 1269-1276, doi:10.1071/Ar05064, 2005.
- 415 Grossiord, C., Gessler, A., Granier, A., Berger, S., Brechet, C., Hentschel, R., Hommel, R., Scherer-Lorenzen, M., and Bonal, D.: Impact of interspecific interactions on the soil water uptake depth in a young temperate mixed species plantation, *J. Hydrol.*, 519, 3511-3519, doi:10.1016/j.jhydrol.2014.11.011, 2014.
- Jesch, A., Barry, K. E., Ravenek, J. M., Bachmann, D., Strecker, T., Weigelt, A., Buchmann, N., de Kroon, H., Gessler, A., Mommer, L., Roscher, C., and Scherer-Lorenzen, M.: Belowground resource partitioning alone cannot explain the biodiversity-ecosystem function relationship: A field test using multiple tracers, *J. Ecol.*, 106, 2002-2018., doi:10.1111/1365-2745.12947, 2018.
- 420



- Martre, P., Cochard, H., and Durand, J.-L.: Hydraulic architecture and water flow in growing grass tillers (*Festuca arundinacea* Schreb.), *Plant Cell Environ.*, 24, 65-76, doi:10.1046/j.1365-3040.2001.00657.x, 2001.
- Meunier, F., Rothfuss, Y., Bariac, T., Biron, P., Durand, J.-L., Richard, P., Couvreur, V., J, V., and Javaux, M.: Measuring and modeling Hydraulic Lift of *Lolium multiflorum* using stable water isotopes, *Vadose Zone J.*, doi:10.2136/vzj2016.12.0134, 2017a.
- 425 Meunier, F., Couvreur, V., Draye, X., Vanderborght, J., and Javaux, M.: Towards quantitative root hydraulic phenotyping: novel mathematical functions to calculate plant-scale hydraulic parameters from root system functional and structural traits, *J. Math. Biol.*, 75, 1133-1170, doi:10.1007/s00285-017-1111-z, 2017b.
- Meunier, F., Draye, X., Vanderborght, J., Javaux, M., and Couvreur, V.: A hybrid analytical-numerical method for solving water flow equations in root hydraulic architectures, *Appl. Math. Model.*, 52, 648-663, doi:10.1016/j.apm.2017.08.011, 2017c.
- 430 Mualem, Y.: A new model predicting the hydraulic conductivity of unsaturated porous media, *Water Resour. Res.*, 12, 513-522, doi:10.1029/WR012i003p00513, 1976.
- Nimah, M. N., and Hanks, R. J.: Model for Estimating Soil-Water, Plant, and Atmospheric Interrelations. 1. Description and Sensitivity, *Soil Sci. Soc. Am. J.*, 37, 522-527, doi:10.2136/sssaj1973.03615995003700040018x, 1973.
- Oerter, E., and Bowen, G.: Spatio-temporal heterogeneity in soil water stable isotopic composition and its ecohydrologic implications in semiarid ecosystems, *Hydrol. Process.*, 33, 1724-1738, doi:10.1002/hyp.13434, 2019.
- 435 Orłowski, N., Breuer, L., and McDonnell, J. J.: Critical issues with cryogenic extraction of soil water for stable isotope analysis, *Ecohydrology*, 9, 3-10, doi:10.1002/eco.1722, 2016.
- Orłowski, N., Breuer, L., Angeli, N., Boeckx, P., Brumbt, C., Cook, C. S., Dubbert, M., Dyckmans, J., Gallagher, B., Gralher, B., Herbstritt, B., Herve-Fernandez, P., Hissler, C., Koeniger, P., Legout, A., Macdonald, C. J., Oyarzun, C., Redelstein, R., Seidler, C., Siegwolf, R., Stumpp, C., Thomsen, S., Weiler, M., Werner, C., and McDonnell, J. J.: Inter-laboratory comparison of cryogenic water extraction systems for stable isotope analysis of soil water, *Hydrol. Earth Syst. Sc.*, 22, 3619-3637, doi:10.5194/hess-22-3619-2018, 2018.
- 440 Parnell, A. C., Phillips, D. L., Bearhop, S., Semmens, B. X., Ward, E. J., Moore, J. W., Jackson, A. L., Grey, J., Kelly, D. J., and Inger, R.: Bayesian stable isotope mixing models, *Environmetrics*, 24, 387-399, doi:10.1002/env.2221, 2013.
- 445 Passot, S., Couvreur, V., Meunier, F., Draye, X., Javaux, M., Leitner, D., Pages, L., Schnepf, A., Vanderborght, J., and Lobet, G.: Connecting the dots between computational tools to analyse soil-root water relations, *J. Exp. Bot.*, 70, 2345-2357, doi:10.1093/jxb/ery361, 2019.
- Rothfuss, Y., and Javaux, M.: Reviews and syntheses: Isotopic approaches to quantify root water uptake: a review and comparison of methods, *Biogeosciences*, 14, 2199-2224, doi:10.5194/bg-14-2199-2017, 2017.
- 450 Schnepf, A., Leitner, D., Landl, M., Lobet, G., Mai, T. H., Morandage, S., Sheng, C., Zorner, M., Vanderborght, J., and Vereecken, H.: CRootBox: a structural-functional modelling framework for root systems, *Ann. Bot.*, 121, 1033-1053, doi:10.1093/aob/mcx221, 2018.
- Schroeder, T., Javaux, M., Vanderborght, J., Korfgan, B., and Vereecken, H.: Implementation of a Microscopic Soil-Root Hydraulic Conductivity Drop Function in a Three-Dimensional Soil-Root Architecture Water Transfer Model, *Vadose Zone J.*, 8, 783-792, doi:10.2136/vzj2008.0116, 2009.
- 455 Schulze, E. D., Mooney, H. A., Sala, O. E., Jobbagy, E., Buchmann, N., Bauer, G., Canadell, J., Jackson, R. B., Loreti, J., Oesterheld, M., and Ehleringer, J. R.: Rooting depth, water availability, and vegetation cover along an aridity gradient in Patagonia, *Oecologia*, 108, 503-511, doi:10.1007/Bf00333727, 1996.



- 460 Sprenger, M., Leistert, H., Gimbel, K., and Weiler, M.: Illuminating hydrological processes at the soil-vegetation-atmosphere interface
with water stable isotopes, *Review of Geophysics*, 54, 674-704, doi:10.1002/2015RG000515, 2016.
- Sulis, M., Couvreur, V., Keune, J., Cai, G. C., Trebs, I., Junk, J., Shrestha, P., Simmer, C., Kollet, S. J., Vereecken, H., and Vanderborght,
J.: Incorporating a root water uptake model based on the hydraulic architecture approach in terrestrial systems simulations, *Agr.
Forest Meteorol.*, 269, 28-45, doi:10.1016/j.agrformet.2019.01.034, 2019.
- 465 van Den Honert, T. H.: Water transport in plants as a catenary process, *Discuss. Faraday Soc.*, 3, 146-153, doi:10.1039/DF9480300146,
1948.
- van Genuchten, M. T.: A closed-form equation for predicting the hydraulic conductivity of unsaturated soils, *Soil Sci. Soc. Am. J.*, 44,
892-898, doi:10.2136/sssaj1980.03615995004400050002x, 1980.
- Volkman, T. H. M., Haberer, K., Gessler, A., and Weiler, M.: High-resolution isotope measurements resolve rapid ecohydrological
dynamics at the soil-plant interface, *New Phytol.*, doi:10.1111/nph.13868, 2016.
- 470 Washburn, E. W., and Smith, E. R.: The isotopic fractionation of water by physiological processes, *Science*, 79, 188-189,
doi:10.1126/science.79.2043.188, 1934.
- Werner, C., Schnyder, H., Cuntz, M., Keitel, C., Zeeman, M. J., Dawson, T. E., Badeck, F. W., Brugnoli, E., Ghashghaie, J., Grams, T. E.
E., Kayler, Z. E., Lakatos, M., Lee, X., Maguas, C., Ogee, J., Rascher, K. G., Siegwolf, R. T. W., Unger, S., Welker, J., Wingate,
L., and Gessler, A.: Progress and challenges in using stable isotopes to trace plant carbon and water relations across scales,
475 *Biogeosciences*, 9, 3083-3111, doi:10.5194/bg-9-3083-2012, 2012.
- Yakir, D., and Sternberg, L. D. L.: The use of stable isotopes to study ecosystem gas exchange, *Oecologia*, 123, 297-311,
doi:10.1007/s004420051016, 2000.



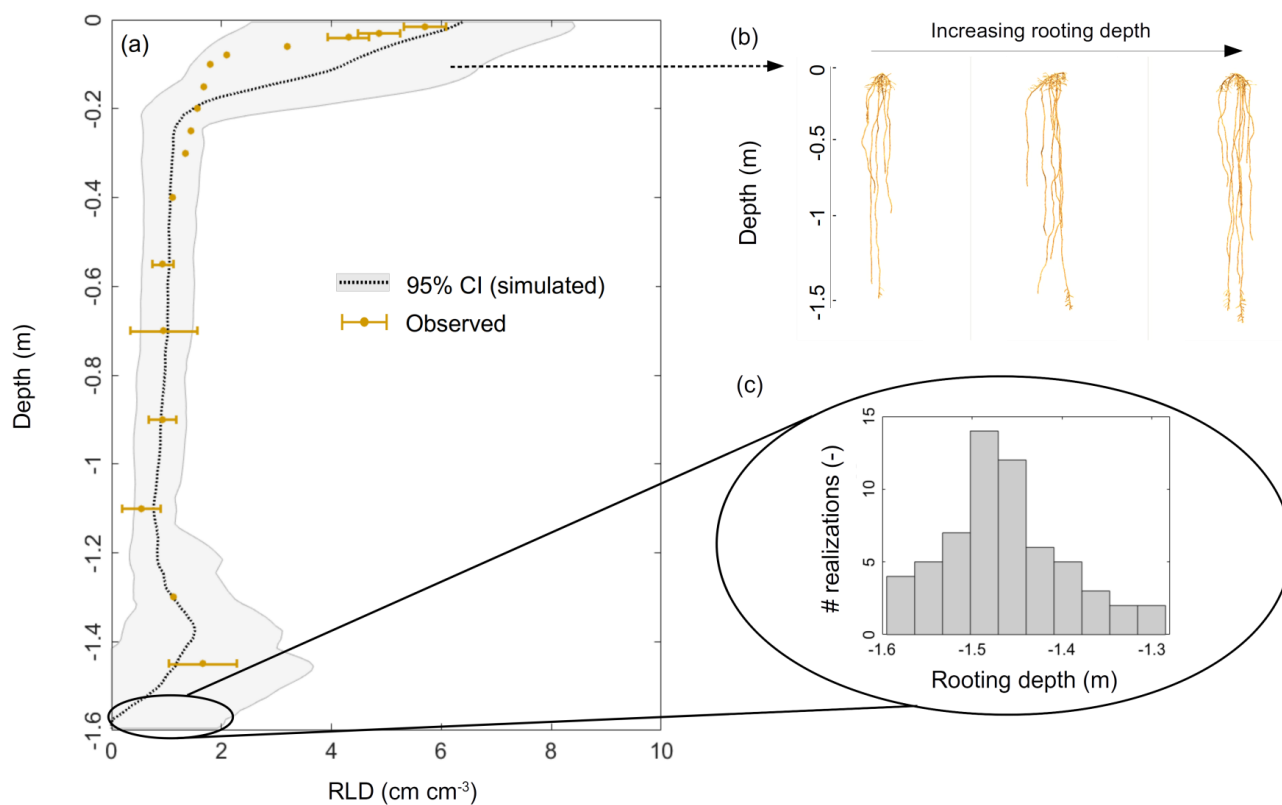
480 **5 Tables**

	L_{pr} (m MPa ⁻¹ s ⁻¹)	k_{axial} (m ⁴ MPa ⁻¹ s ⁻¹)	k_{sat} (m ² MPa ⁻¹ s ⁻¹)	λ (-)
Lower limit	10^{-11}	10^{-13}	10^{-5}	-5
Upper limit	10^{-6}	10^{-8}	10^{-2}	2
Value at best fit	$2.3 \cdot 10^{-7}$	$4.5 \cdot 10^{-11}$	$9.5 \cdot 10^{-3}$	-4.9

Table 1. Optimum and limits of the four-dimensional parametric space explored by the global optimization algorithm aiming at minimizing the difference between simulated and observed δ_{tiller} and ψ_{leaf} , as well as their standard deviation from average values during the full experiment.



6 Figures



485

Figure 1. (a) Simulated (grey envelopes) and observed (brown dots) root length density profiles. Panels (b) and (c) illustrate the variability in modelled root system architectures and rooting depths, respectively.

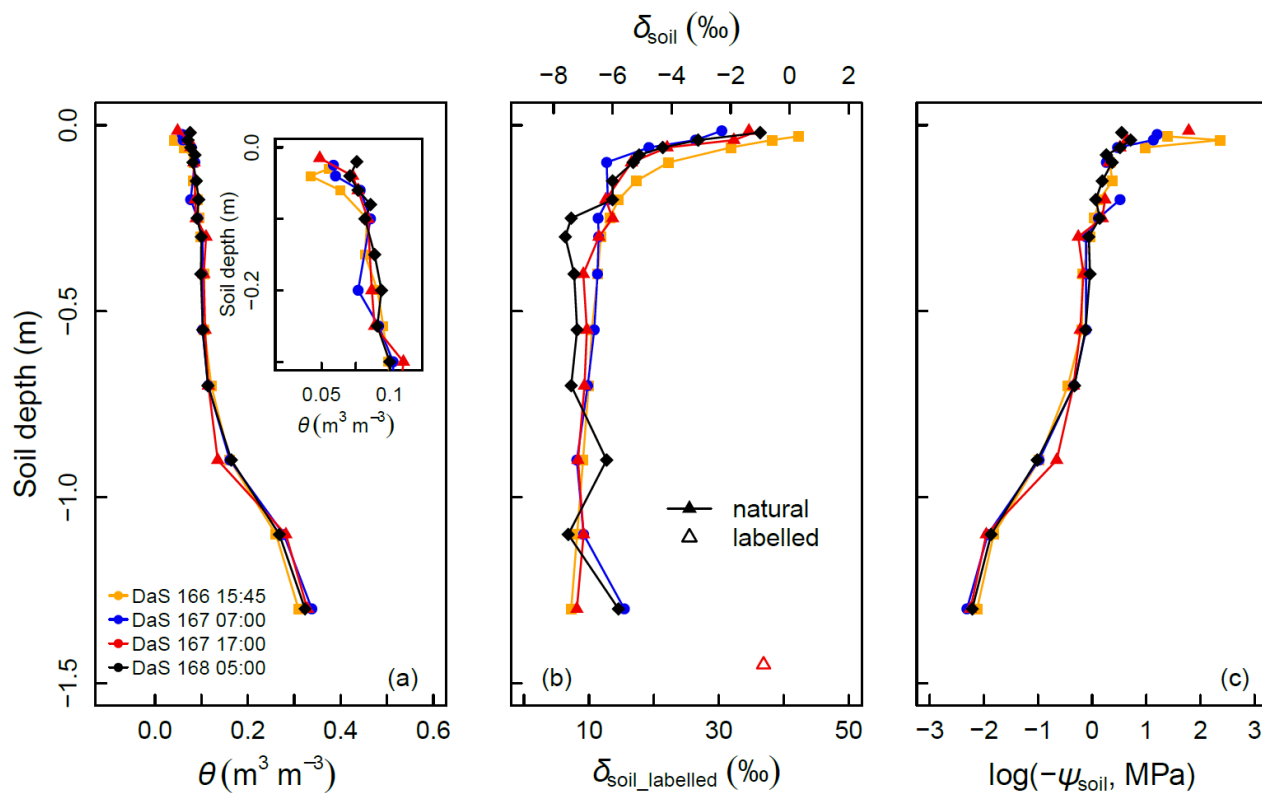


Figure 2. Soil volumetric water content (θ , panel a), oxygen isotopic composition (δ_{soil} , panel b), and calculated soil matric potential (ψ_{soil} , panel c) profiles during the sampling period.

490

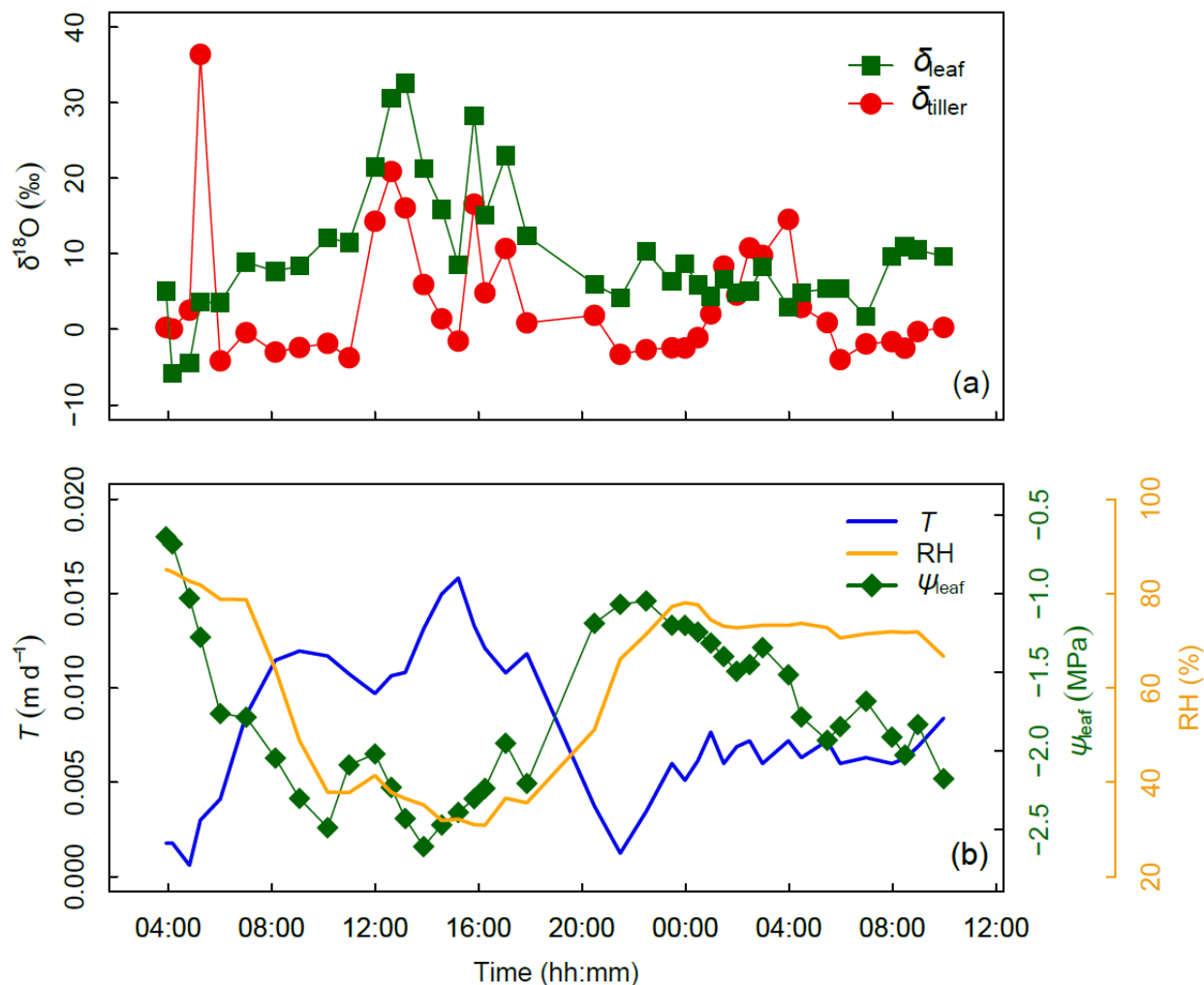


Figure 3. (a) Time series of tiller and leaf water oxygen isotopic compositions (δ_{tiller} and δ_{soil} , ‰). (b) Transpiration flux (T , in m d^{-1}), relative humidity (RH, %), and leaf water potential (ψ_{leaf} , in MPa, panel b) from days after seeding DaS 167 – 04:00 to DaS 168 – 11:00. Time of Labeling was DaS 166 – 17:00.

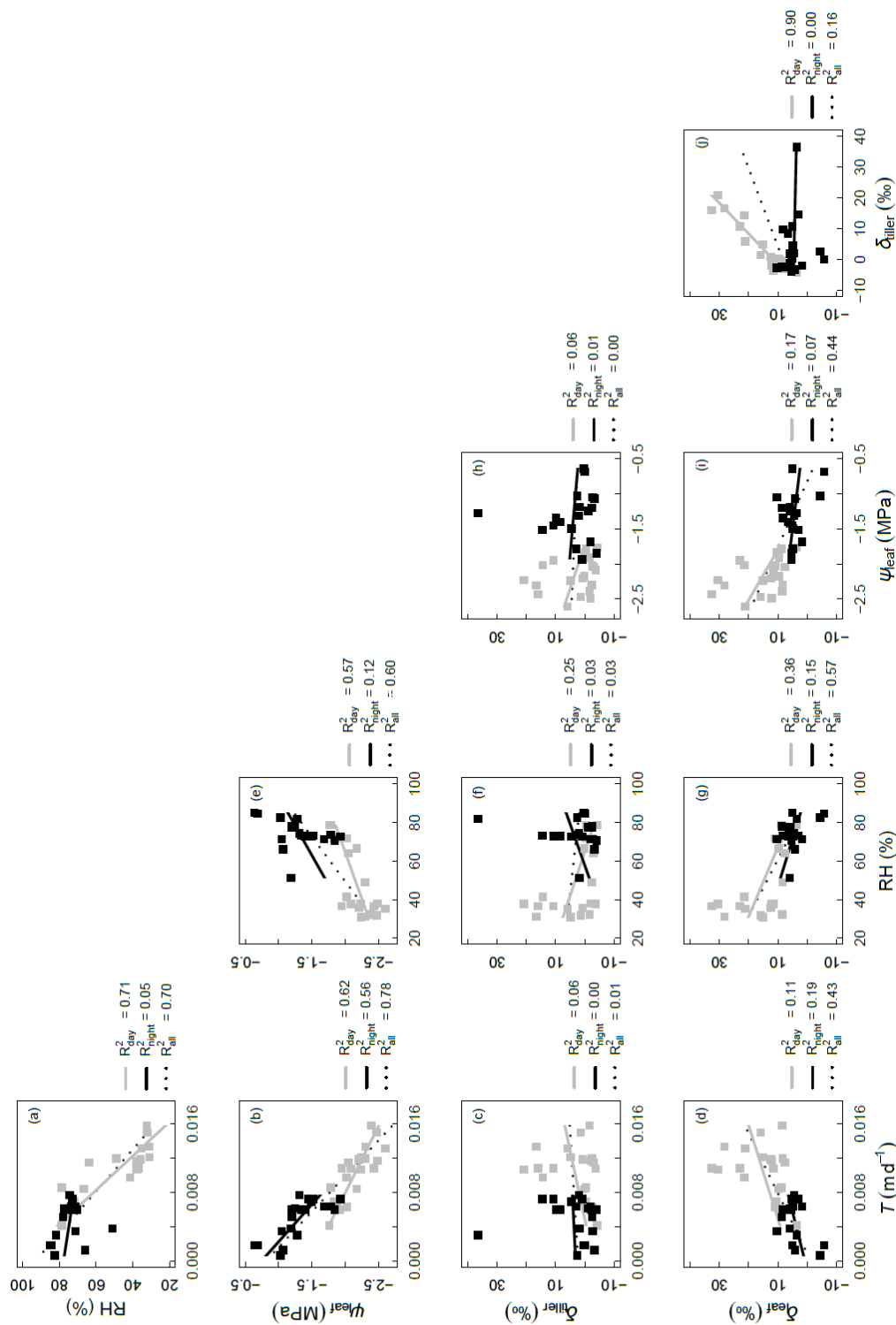
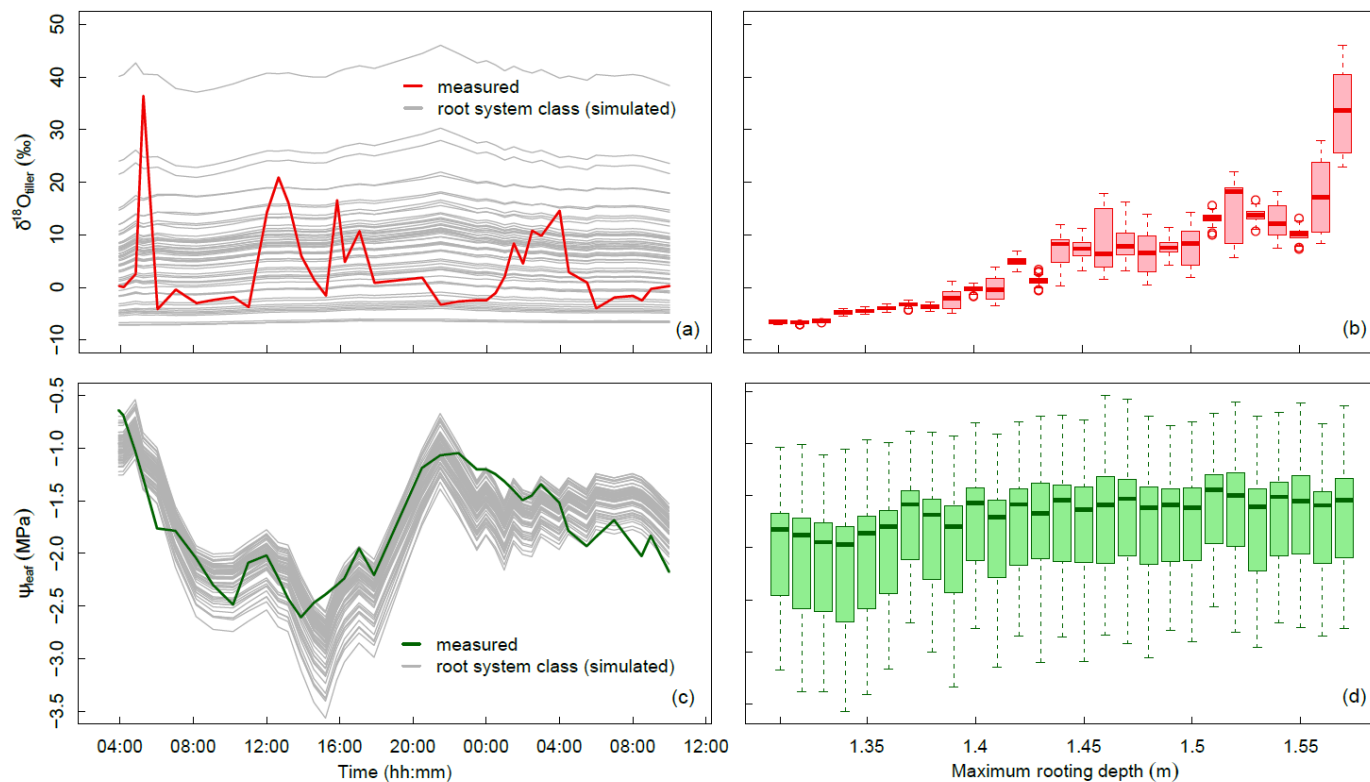


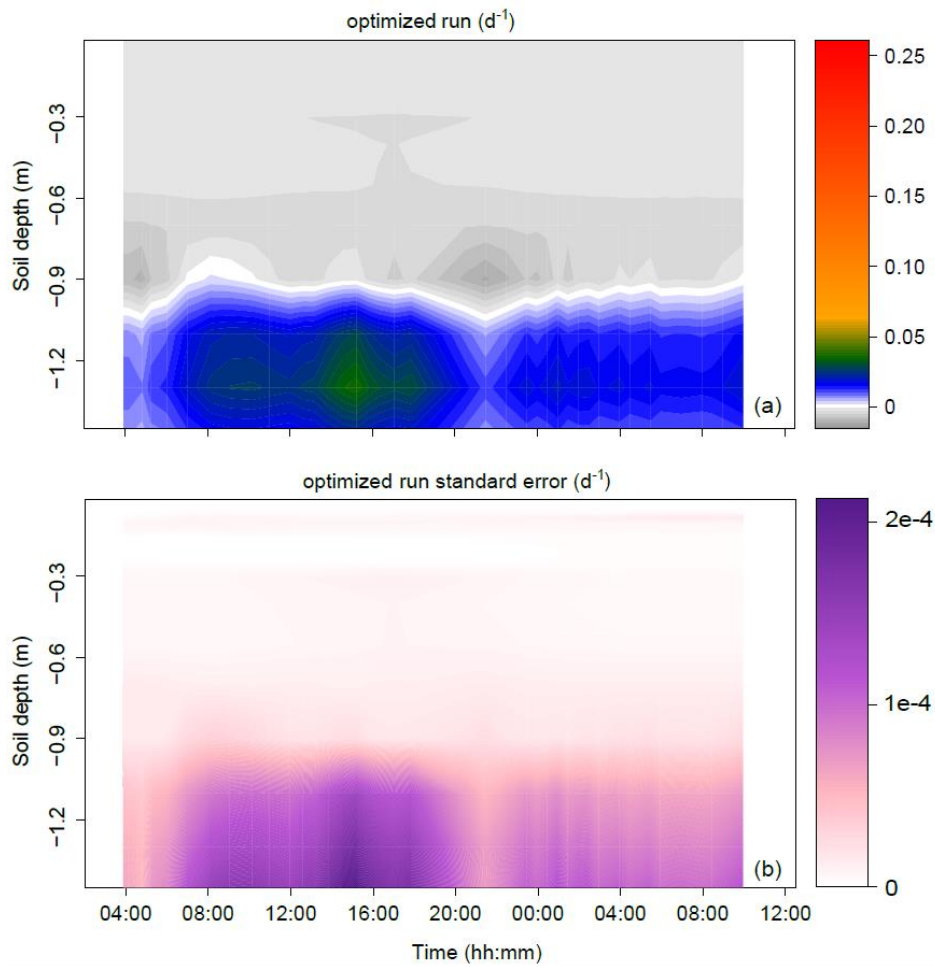
Figure 4. Correlations between measured variables: oxygen isotopic compositions of xylem and leaf waters (δ_{filler} and δ_{leaf}), transpiration rate (T , in m d^{-1}), relative humidity (RH, %), and leaf water potential (ψ_{leaf} in MPa). Coefficient of determinations (R^2) are reported for all data, and separately for ‘day’ data (gray symbols) and ‘night’ data (black symbols) (see Appendix C for definition of ‘day’ and ‘night’ experimental periods).

1
 2
 3
 4



1

2 **Figure 5. Variation of δ_{tiller} and ψ_{leaf} in time and across the 60 classes of simulated root systems. (a) Temporal dynamics of δ_{tiller}**
3 **measured (thick red line) and simulated (thin grey lines, one line per root system class). (b) Boxplot of simulated δ_{tiller} values for**
4 **each root system maximum depth, by 1 cm increment. (c) Temporal dynamics of ψ_{leaf} measured (thick green line) and simulated**
5 **(thin grey lines, one line per root system class). (d) Boxplot of simulated ψ_{leaf} values for each root system maximum depth, by 1 cm**
6 **increment.**



1

2

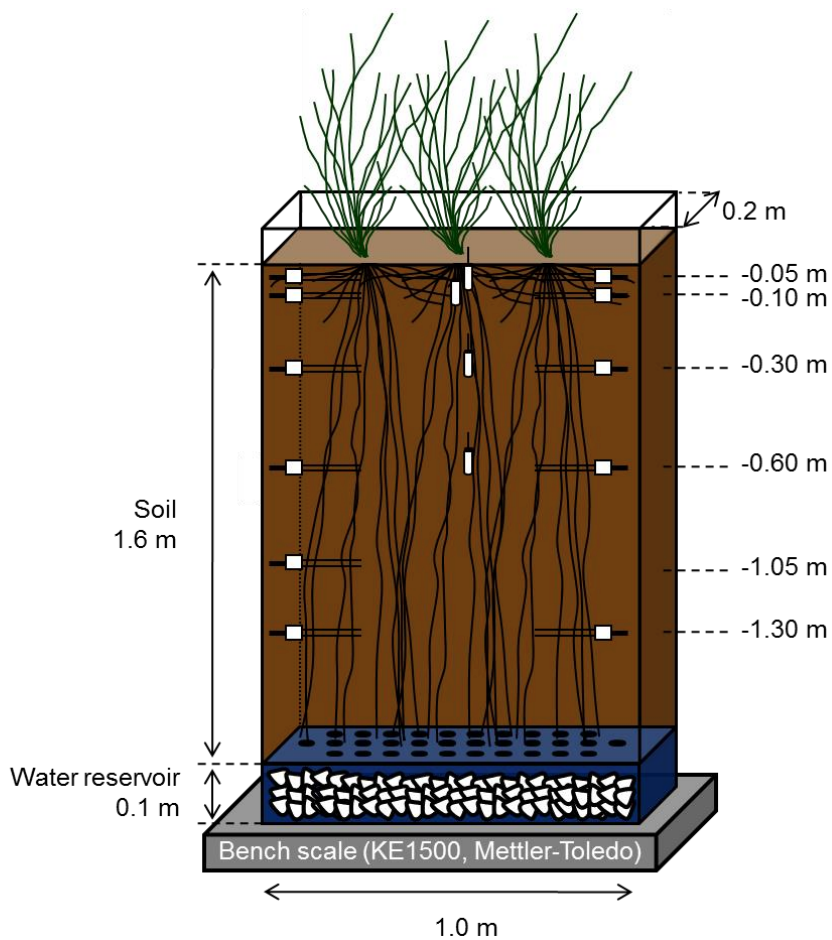
3

4

Figure 6. Time series of the profiles of root water uptake per unit soil volume (sink term, d^{-1}) computed with the physically-based model. (a) Average sink terms across the 60 classes of the population. (b) Variability within the 60 classes of the population (1 standard deviation).



1 7 Appendix



-  Tensiometer (SMS 2000, SDEC)
-  Soil volumetric water content reflectrometers (CS616, Campbell Sci.)

2
3 Appendix A. Soil macro-rhizotron experimental setup with tall fescue cover



$\theta_{\text{sat}} (\text{m}^3 \text{ m}^{-3})$	$\theta_{\text{res}} (\text{m}^3 \text{ m}^{-3})$	$\alpha (\text{m}^{-1})$	$n (-)^1$
0.4	0.044	0.0285	2.29

2 **Appendix B. Soil retention curve and parameters optimized values (van Genuchten, 1980 - Burdine) (Meunier et al., 2017a)**



1 Appendix C. Timeline of destructive sampling

DAS 167		'day' data												'night data'														
Time		15:45	03:55	04:10	04:50	05:15	06:00	07:00	08:10	09:05	10:10	11:00	12:00	12:40	13:10	13:55	14:35	15:15	15:50	16:15	17:00	17:50	20:30	21:30	22:30	23:30		
Soil	x						x															x						
Leaves		x	x	x	x	x	x	x	x	x	x	x	x	x	x	x	x	x	x	x	x	x	x	x	x	x	x	
roots	x																											
DAS 168		'night data'												'day' data														
Time		00:00	00:30	01:00	01:30	02:00	02:30	03:00	04:00	04:30	05:00	05:30	06:00	07:00	08:00	08:30	09:00	10:00										
Soil											x																	
Leaves	x	x	x	x	x	x	x	x	x	x																		



Appendix D. Inverse modeling scheme

The parametrization method was inverse modeling, with four targets: (i) minimizing the differences between observed and predicted δ_{tiller} in each pool p , (ii) minimizing the difference between the standard deviations of observed and predicted δ_{tiller} (temporal and population deviations altogether), (iii) minimizing the differences between observed and predicted ψ_{leaf} in each root system class i , (iv) minimizing the difference between the standard deviations of observed and predicted δ_{tiller} (temporal and population deviations altogether). These targets translated as an objective function (OF) to be minimized, where differences were normalized by the standard deviation (SD) of observations in order to make the error function dimensionless:

$$OF = \sqrt{\frac{1}{2} \left(\frac{1}{N_p N_t} \sum_i \sum_t \left(\frac{\delta_{\text{tiller,obs}}(t) - \delta_{\text{tiller,p,sim}}(t)}{SD(\delta_{\text{tiller,obs}}(t))} \right)^2 + \frac{1}{N_i N_t} \sum_i \sum_t \left(\frac{\psi_{\text{leaf,obs}}(t) - \psi_{\text{leaf,i,sim}}(t)}{SD(\psi_{\text{leaf,obs}}(t))} \right)^2 \right)} + \left| \frac{SD(\delta_{\text{tiller,obs}}(t)) - SD(\delta_{\text{tiller,p,sim}}(t))}{SD(\delta_{\text{tiller,obs}}(t))} \right| + \left| \frac{SD(\psi_{\text{leaf,obs}}(t)) - SD(\psi_{\text{leaf,i,sim}}(t))}{SD(\psi_{\text{leaf,obs}}(t))} \right| \quad (D1)$$

where N_p is the number of δ_{tiller} pools simulated (100) at each observation time, N_i is the number of plant classes simulated (60), and N_t the total number of observation times (40).

The global optimizer Multistart heuristic algorithm OQNLP (Optimal Methods Inc.) of the MATLAB (The MathWorks, Inc., USA) optimization toolbox was used to minimize the error function within the lower and upper limits of the parametric space reported in Table 1.



Appendix E. Statistical determination of relative RWU profiles with SIAR

The Bayesian inference statistical model SIAR (Parnell et al., 2013) was used to determine the profiles of relative contributions to RWU (rRWU, dimensionless) of ten identified potential water sources. These water sources were defined to originate from the soil layers 0.00-0.03, 0.03-0.07, 0.07-0.15, 0.15-0.30, 0.30-0.60, 0.60-0.90, 0.90-1.20, 1.20-1.32, 1.32-1.37, and 1.37-1.44 m. Their corresponding isotopic compositions were obtained from the measured soil water isotopic compositions (δ_{soil}) and volumetric content (θ) values following Eq. (E1) (Rothfuss and Javaux, 2017):

$$\delta_{\text{soil},J} = \frac{\sum_{j \in J} \delta_{\text{soil},j} \cdot \theta_j \cdot \Delta Z_j}{\sum_{j \in J} \theta_j \cdot \Delta Z_j} \quad (\text{E1})$$

where J is the soil layer index, j is the soil sub-layer index, and ΔZ_j is the thickness of the soil sub-layer j. Therefore, equation (E1) translates the soil water isotopic composition measured across sub-layers j into representative isotopic compositions of the different sources (i.e., across layers J). The computed $\delta_{\text{soil},J}$ were compared to δ_{tiller} values. For this, δ_{tiller} measurements were pooled in twelve groups corresponding to different time periods. These groups were defined to best reflect the apparent temporal dynamics of δ_{tiller} .

For each of the twelve time periods:

- (i) the function `siarmcmcdirichletv4` of the SIAR R package (<https://cran.r-project.org/web/packages/siar/index.html>) was run 500,000 times with prescribed burnin and thinby equal to 50000 and 15, respectively. The output of the model (i.e., the *a posteriori* rRWU distribution across the ten soil water sources J) was obtained from a flat Dirichlet *a priori* rRWU distribution (i.e., $\text{rRWU}_j=1/10$);
- (ii) the ‘best run’ (*br*, dimensionless) was selected from SIAR’s output. It was defined as the closest solution of relative contributions across sources from the set of most frequent values (*mfv*, dimensionless), i.e., the relative contribution with the greatest probability of occurrence. The best run was identified as minimizing the objective function below, i.e., the RMSE (root mean square error) with respect to the set of mfv_j :

$$OF = \sqrt{\frac{\sum_{j=1}^{10} (\text{mfv}_j - \text{br}_j)^2}{10}} \quad (\text{E2})$$

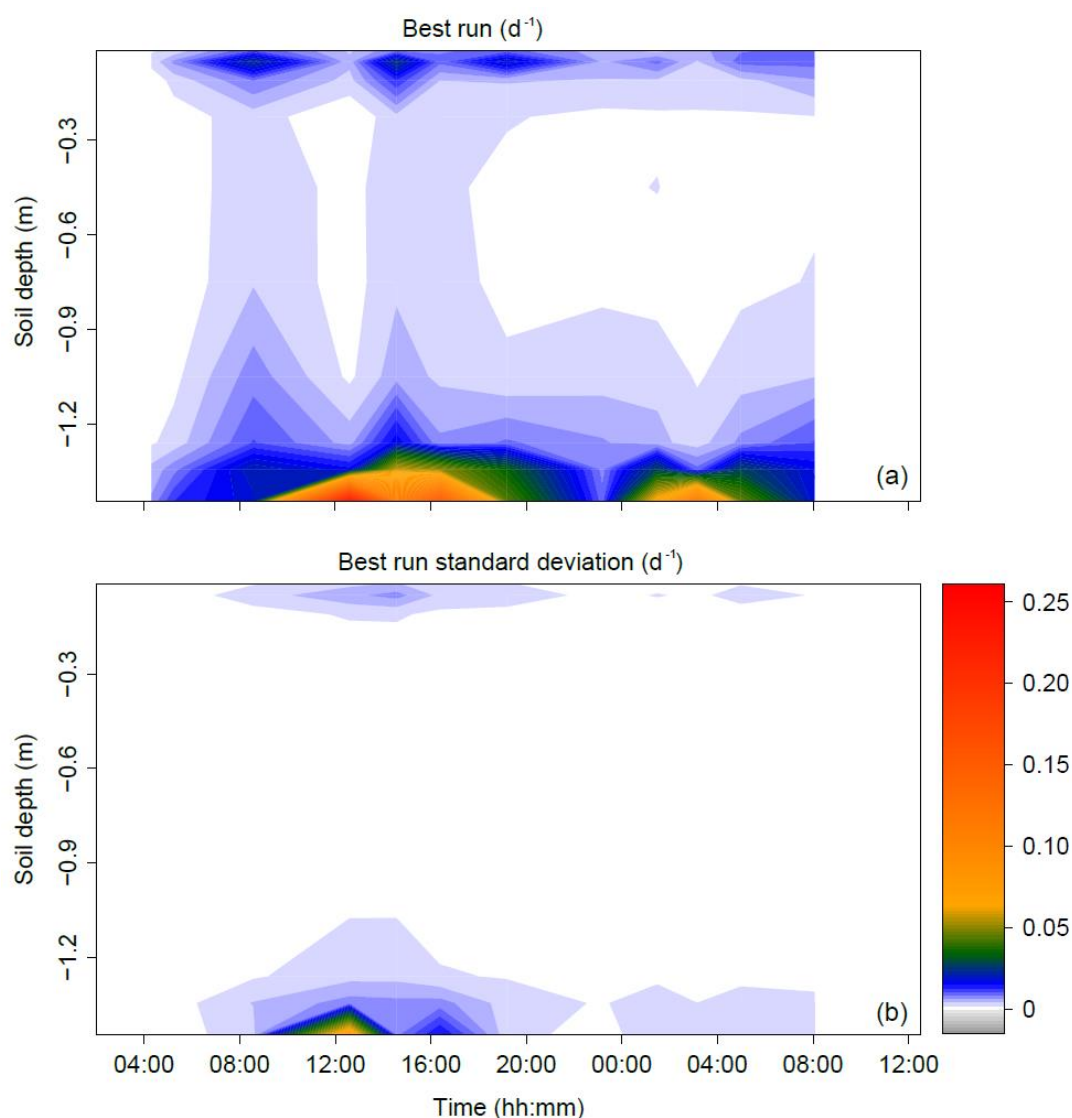


40

(iii) br was then multiplied by transpiration rate (in m d^{-1}) and divided by soil layer thicknesses (ΔZ_j , in m) to obtain sink terms (S_j , i.e. root water uptake rate per unit soil volume, expressed in d^{-1}). The interest of sink terms in a comparison is that they do not vary with soil vertical discretization.

Steps (i)-(iii) were repeated a 1,000 times to estimate the variance of the best run for each time period and soil water source

J.



45 Figure E. Time series of the profiles of root water uptake per unit soil volume (sink term, d^{-1}) computed with the statistical model SIAR (a). Panel (b) reports the variance of the estimated sink term (1 standard deviation).